UNIVERSIDADE TECNOLÓGICA FEDERAL DO PARANÁ
PROGRAMA DE PÓS-GRADUAÇÃO EM ENGENHARIA ELÉTRICA E INFORMÁTICA INDUSTRIAL

DIOGO NOGUEIRA KNOP

REPLICAÇÃO DE CABEÇALHOS CODIFICADOS EM REDES LR-FHSS

DISSERTAÇÃO

CURITIBA
2024

DIOGO NOGUEIRA KNOP

REPLICAÇÃO DE CABEÇALHOS CODIFICADOS EM REDES LR-FHSS

LR-FHSS Networks with Coded Header Replication

Dissertação apresentada como requisito para obtenção do título de Mestre em Engenharia Elétrica e Informática Industrial, do Programa de Pós-Graduação em Engenharia Elétrica e Informática Industrial, da Universidade Tecnológica Federal do Paraná (UTFPR).

Orientador: Prof. Dr. João Luiz Rebelatto
Coorientador: Prof. Dr. Richard Demo Souza

CURITIBA

2024

Ministério da Educação
Universidade Tecnológica Federal do Paraná
Campus Curitiba

DIOGO NOGUEIRA KNOP

REPLICAÇÃO DE CABEÇALHOS CODIFICADOS EM REDES LR-FHSS

Trabalho de pesquisa de mestrado apresentado como requisito para obtenção do título de Mestre Em Ciências da Universidade Tecnológica Federal do Paraná (UTFPR). Área de concentração: Telecomunicações E Redes.

Data de aprovação: 23 de Abril de 2024

Dr. Joao Luiz Rebelatto, Doutorado - Universidade Tecnológica Federal do Paraná

Dr. Jamil De Araujo Farhat, Doutorado - Universidade Tecnológica Federal do Paraná

Dr. Jean Michel De Souza Sant Ana, Doutorado - University Of Oulu

Dr. Richard Demo Souza, Doutorado - Universidade Federal de Santa Catarina (Ufsc)

To my dear wife,

For your unwavering love and endless support, this thesis is dedicated to you. Your encouragement has been my strength throughout this journey.

ACKNOWLEDGEMENTS

I am grateful to my beloved family, whose unwavering support and endless encouragement made this journey possible. Your love has been my guiding light through every challenge.

To my esteemed advisor, Professor João Luiz Rebelatto, your guidance, belief, and constant striving for excellence never let me waver. His guidance has been invaluable, shaping my academic and personal growth. Thank you for never disappointing me.

The inventor... looks upon the world and is not contented with things as they are. He wants to improve whatever he sees, he wants to benefit the world (BELL, Alexander Graham, 1891).

RESUMO

KNOP, Diogo Nogueira. **Replicação de Cabeçalhos Codificados em Redes LR-FHSS**. 2024. 51 f. Dissertação (Mestrado em Engenharia Elétrica e Informática Industrial) – Universidade Tecnológica Federal do Paraná. Curitiba, 2024.

Espalhamento Espectral por Salto de Frequência de Longo Alcance (LR-FHSS, do inglês *Long-Range Frequency-Hopping Spread Spectrum*) foi recentemente introduzido no contexto de redes LoRaWAN, com o objetivo de mitigar colisões de pacotes e aumentar a capacidade da rede. Isso é alcançado replicando cabeçalhos e fragmentando pacotes de dados em segmentos menores, distribuídos aleatoriamente por vários canais para melhorar a resiliência contra interferências. Estudos recentes no escopo de LR-FHSS destacaram a importância das taxas de erro de cabeçalho na determinação do erro geral do sistema, indicando as limitações dos códigos de repetição tradicionais para correção de erros. Nesse sentido, esta dissertação propõe um esquema de combinação inter-cabeçalho baseado em códigos de rede para melhorar a proteção do cabeçalho contra apagamentos e colisões. Por meio de investigações analíticas e baseadas em simulação, o estudo demonstra uma redução substancial nas taxas de erro de pacotes de mais de uma ordem de magnitude em vários cenários, destacando a eficácia do esquema proposto em melhorar a confiabilidade em implantações de LoRaWAN.

Palavras-chave: Códigos Corretores de Erros. Internet-das-Coisas. LoRa. LoRaWAN. LR-FHSS.

ABSTRACT

KNOP, Diogo Nogueira. **LR-FHSS Networks with Coded Header Replication**. 2024. 51 p. Dissertation (Master's Degree in Electrical and Computer Engineering) – Universidade Tecnológica Federal do Paraná. Curitiba, 2024.

Long-Range Frequency-Hopping Spread Spectrum (LR-FHSS) has recently been introduced within the Long Range Wide Area Network (LoRaWAN) framework, aiming to mitigate packet collisions and enhance network capacity. This is achieved by replicating headers and segmenting data packets into smaller fragments randomly distributed across multiple channels to improve resilience against interference. Recent research within the LR-FHSS domain has highlighted the significance of header error rates in influencing the overall system error, indicating the limitations of traditional repetition codes for error correction. In response, this thesis proposes a network-coded-aided inter-header combination scheme to enhance header protection against both erasures and collisions. Through analytical and simulation-based investigations, the study demonstrates a substantial reduction in packet error rates by more than one order of magnitude across various scenarios, underscoring the effectiveness of the proposed scheme in enhancing reliability and resilience in LoRaWAN deployments.

Keywords: Error Correcting Codes. Internet-of-Things. LoRa. LoRaWAN. LR-FHSS.

LIST OF FIGURES

LIST OF TABLES

LIST OF ACRONYMS

INITIALISM

CR	Coding Rate
CSS	Chirp Spread Spectrum
D2D	Device to Device
DFH	Dynamic Frequency Hopping
DR	Data Rate
DtS	Direct-to-Satellite
DtS-IoT	Direct-to-Satellite Internet of Things
ECC	Error Correcting Code
ED	End-Device
ETSI	European Telecommunications Standards Institute
FHS	Frequency Hopping Sequences
FHSS	Frequency Hopping Spread Spectrum
GW	Gateway
IoT	Internet of Things
IP	Internet Protocol
LEO	Low Earth Orbit
LoRa	Long Range
LoRaWAN	Long-Range Wide-Area Network
LOS	Line-of-Sight
LPWAN	Low-Power Wide-Area Network
LR-FHSS	LoRa-Frequency Hopping Spread Spectrum
LR-FHSS-NC	Network Coding-aided LR-FHSS
M2M	Machine to Machine
MAC	Medium Access Control
MDS	Maximum-Distance Separable
NC	Network Coding
NCC-LoRa	Network-Coded Cooperation Long Range
NS	Network Server
OBW	Occupied Bandwidth
OCW	Occupied Channel Width
PEP	Packet Error Probability
PER	Packet Error Rate
PRGN	Pseudo-Random Number Generator

PRR	Packet Reception Rate
RS	Reed-Solomon
RT-LoRa	Long Range with Retransmissions
SF	Spreading Factor
SNR	Signal-to-Noise Ratio
ToA	Time-on-Air

LIST OF SYMBOLS

LATIN LETTERS

δ	Amount of accumulated packets for combining
ϵ	Erasure probability
γ	Minimum payload fragment necessary for decoding
$\mathcal{P}_{\text{hour}}$	Average packets/hour/device
$\mathcal{S}_{\text{F}}$	SF
S	Receiver sensitivity
$\mathrm{ToA}_{\text{LoRa}}$	Duration of a packet (time-on-air) LoRa
ToA_{LR}	Duration of a packet (time-on-air) LR-FHSS
μ	Average inter-arrival time of packet elements within one hour
μ_{H}	Average inter-arrival time of header elements within one hour
μ_{L}	Average inter-arrival time of payload elements within one hour
Ψ	Minimum LoRa reception signal-to-noise ratio
ρ	Maximum duty cycle
PL	Payload length, in bytes
A_{H}	Average number of packet elements arriving at the gateway during a header transmission
A_{L}	Average number of packet elements arriving at the gateway during a payload transmission
B	Bandwidth
C	Carriers for FH per OCW channel
CR	CR
Frx	Received payload fragment counter
Hrx	Received header counter
n_{pay}	Number of LoRa payload symbols
n_{pre}	Number of LoRa preamble symbols
N_H	Number of transmitted PHY header replicas
N_L	Number of payload fragments
P_{H}	Probability of correctly receiving header
P_{L}	Probability of correctly receiving payload
p_{error}	Error probability
p_{success}	Success probability
$p_{\text{success}}^{\text{NC}}$	LR-FHSS-NC packet success probability
R	Payload error correcting code rate
R_b	LoRa transmission rate, in bits/s
T_{frag}	Fragment payload period
ToA	Duration of a packet (time-on-air)
$DE\left(\mathcal{S}_{\text{F}}\right)$	Low rate optimization function

CONTENTS

1 INTRODUCTION

Internet of Things (IoT) is regarded as the third major wave in information technology, succeeding the internet and mobile communications. IoT relies on a substantial infrastructure consisting of potentially numerous connected devices, with Machine to Machine (M2M) communications representing a rapidly growing market (NOLAN *et al.*, 2016). The concept of IoT has garnered substantial attention and research in recent years, as its implications span a wide range of domains. In the field of healthcare, IoT-integrated medical devices can persistently observe patients' vital signs, offering early alerts of health complications and enabling remote diagnosis and treatment (ATZORI *et al.*, 2010). In the agricultural sector, IoT sensors and actuators provide precision farming methods, optimizing resource consumption and crop production (AHMED *et al.*, 2019). The transportation industry gains from IoT via improved vehicle tracking, traffic control, and the advancement of autonomous vehicles (CHEN *et al.*, 2018). Furthermore, the integration of IoT into our daily lives extends to smart homes, where interconnected appliances and systems offer greater convenience, energy efficiency, and security (BORGIA, 2014). IoT also plays a pivotal role in the evolution of smart cities, where interconnected infrastructure enhances urban services, sustainability, and citizen well-being (AL-FUQAHA *et al.*, 2015).

Low-Power Wide-Area Network (LPWAN)s are gaining attention due to their ability to provide affordable connectivity to low-power devices distributed across large geographic areas. These networks play a crucial role in realizing the vision of the IoT, where they complement and sometimes replace conventional cellular and short-range wireless technologies for various emerging smart city and M2M applications (RAZA *et al.*, 2017). Long Range (LoRa) technology is one leading LPWANs, outperforming other LPWAN technologies in terms of signal propagation (IKPEHAI *et al.*, 2019). One of the key advantages of LoRa is its low power consumption, making it suitable for battery-operated IoT devices, which can operate on a single battery charge for several years, thanks to their efficient power management and the ability to transmit data at different data rates (RAZA *et al.*, 2017). Based on the Chirp Spread Spectrum (CSS) modulation technique (SELLER, 2017), LoRa offers exceptional coverage and penetration capabilities, making it ideal for connecting remote and battery-powered devices (ATZORI *et al.*, 2010). CSS modulation spreads the signal across a wide bandwidth, allowing LoRa devices to communicate over several kilometers in urban environments and even farther in rural areas (ATZORI *et al.*, 2014). This long-range capability is crucial for applications such as smart agriculture, environmental monitoring, and asset tracking.

Moreover, the LoRa Alliance has developed the Long-Range Wide-Area Network (LoRaWAN) protocol, widely adopted for network implementations utilizing LoRa technology. LoRaWAN complements LoRa's physical layer with a robust network protocol designed to manage large-scale IoT deployments. Usually, LoRa networks operate with one link between the End-Device (ED) and the Gateway (GW), however, there's an option for signal relay (LORA ALLIANCE, INC., 2017). There is no direct connection between them, therefore, it's possible that an additional gateway within the coverage area could receive the signal transmitted by the device. Additionally, it employs an access scheme based on ALOHA for communication, lacking collision avoidance mechanisms (SUNDARAM *et al.*, 2020).

Despite its widespread adoption, LoRaWAN faces scalability challenges primarily due to the collision-prone ALOHA protocol in its Medium Access Control (MAC) layer. This deficiency exposes LoRaWAN to collision risks, making it less effective in managing high-density deployments and compromising global scalability. This issue, coupled with LoRaWAN's significant commercial adoption, has motivated numerous recent research endeavors. These efforts include network behavior modeling (GEORGIOU; RAZA, 2017; MAHMOOD *et al.*, 2019), as well as innovative approaches to enhance system performance proposed (HOELLER *et al.*, 2018; SANT'ANA *et al.*, 2020; SANT'ANA *et al.*, 2020; ALVES *et al.*, 2022).

Semtech has introduced a significant advancement in the LoRa ecosystem with the release of LoRa-Frequency Hopping Spread Spectrum (LR-FHSS), a new physical layer used for uplink messages on LoRaWAN (LORA ALLIANCE, INC., 2021). This latest addition, highlighted in the most recent version of the LoRa Alliance specification, aims to further enhance LoRaWAN networks, bringing fast frequency hopping spread spectrum capabilities to LoRa. Recent studies LR-FHSS's role in enhancing the scalability and reliability of LoRaWAN networks, particularly in scenarios involving satellite connectivity and large-scale deployments of reporting devices with infrequent transmissions (BOQUET *et al.*, 2021; ULLAH *et al.*, 2022a).

In LR-FHSS, header replicas and payload fragments are transmitted independently, such that the gateway needs to correctly recover at least one header replica and a certain amount of payload fragments in order for the packet to be correctly decoded. However, despite the potential increase in the number of supported devices, recent works have shown that the header replica error rate dictates the overall error performance of LR-FHSS networks (ULLAH *et al.*, 2022a).

1.1 CONTRIBUTION

In this work, we elaborate on the LR-FHSS protocol by proposing an inter-hader coding scheme, based on the concept of Network Coding (NC). The proposed scheme, hereafter referred to as Network Coding-aided LR-FHSS (LR-FHSS-NC), improves the header protection by coding multiple headers from different packets of the same ED through NC, as discussed in (XIAO; SKOGLUND, 2010) and (REBELATTO *et al.*, 2012), prior the transmission to the gateway.

The outage probability of LR-FHSS-NC is formulated with the aid of the model developed in (MALEKI *et al.*, 2023a). The analytical and simulated results of LR-FHSS-NC are compared to the benchmark LR-FHSS scheme, showing that significant improvements can be achieved.

1.2 MOTIVATION

This research is motivated by the increasing importance of LPWANs, particularly with LoRa networks leading the way in this technological advancement. These networks offer the potential to connect numerous IoT devices, supporting various applications like smart cities, precision agriculture, industrial automation, and environmental monitoring.

Despite their impressive capabilities, LoRa networks face challenges, especially in challenging radio frequency (RF) environments commonly encountered in real-world IoT deployments. Issues like channel fading and interference can lead to packet errors, compromising the reliability and effectiveness of LoRa networks and limiting their potential impact. More specifically, exploring network coding within the LR-FHSS context is an alternative to improve the header's protection against errors and collisions.

Through this thesis, we aim to show the benefits and practical implementation considerations of network coding in LR-FHSS networks. By doing so, we seek to contribute to the existing body of knowledge in this field, provide valuable insights to researchers and practitioners, and ultimately advance the capabilities of LoRa networks for a wide range of IoT applications. Our motivation stems from the belief that network coding can unleash the full potential of LoRa networks, further enhancing their impact on shaping the future of IoT.

1.3 OBJECTIVES

In this work, we build upon the LR-FHSS model proposed by (ULLAH *et al.*, 2022a) by considering an inter-header combining scheme, where multiple packets' header replicas from the same user are effectively combined to improve error performance over an erasure channel. More specifically, the contributions of this work can be summarized as follows:

- We propose an inter-header coding scheme to be used in LR-FHSS. Specifically, in the proposed scheme, which we refer to as LR-FHSS-NC, the headers of multiple packets from the same user are combined using Maximum-Distance Separable (MDS) error-correcting codes (REBELATTO *et al.*, 2012).
- Through mathematical analysis and simulation results, we demonstrate that LR-FHSS-NC can achieve higher levels of reliability in exchange for increased delay, without requiring additional bandwidth or transmission power resources.

1.4 PUBLISHED PAPERS

The following paper has been published with the results of this work (KNOP *et al.*, 2024):

- D. N. Knop, J. L. Rebelatto and R. D. Souza, "LR-FHSS with Network-Coded Header Replication," in *IEEE Transactions on Vehicular Technology*, 2024.
  DOI: 10.1109/TVT.2024.3350635

1.5 DOCUMENT STRUCTURE

The rest of this thesis is structured as follows. Chapter 2 provides a detailed review of the literature that covers recent advances relevant to the topic explored in this research. In Chapter 3, fundamental concepts related to the system model are introduced, outlining the standard LR-FHSS scheme. Chapter 4 details the proposed scheme, with a focus on its outage probability, along with the description of the simulator and analytical model. This section examines the impact of NC on LR-FHSS. Moving on to Chapter 5, simulation results are compiled, offering a comprehensive analysis of observed behaviors. Finally, Chapter 6 presents conclusions drawn from the study's findings and suggests directions for future research.

2 LITERATURE REVIEW

The pioneering work of (BOQUET *et al.*, 2021) presents an initial LR-FHSS performance analysis, providing an overview of its specification, the format of the physical layer packets, and the frequency hopping strategy. Their innovative approach was underpinned by the development of a robust simulator, which was instrumental in validating their theoretical constructs. The study highlights a significant potential advantage of LR-FHSS over LoRaWAN CSS in dense network scenarios. The study yielded significant results, demonstrating the superior network scalability of LR-FHSS compared to LoRa DR0. Specifically, the 162 bps LR-FHSS data rates provided two orders of magnitude more network capacity while maintaining the same radio link budget as LoRa DR0 (SF12). Importantly, LR-FHSS retained the long-range communication characteristics of LoRa, making it suitable for both terrestrial and satellite deployments. However, it is essential to note that (BOQUET *et al.*, 2021) only considers packet collisions based on simultaneous transmissions selecting the same subcarrier and coinciding in time, neglecting other factors such as channel impairments and path loss, which also impact LR-FHSS performance.

In (ULLAH *et al.*, 2022a), the authors provide one of the first studies on LR-FHSS for Direct-to-Satellite (DtS) scenario, by developing analytical and simulation models to characterize the packet delivery probability of LR-FHSS. The analytical model derives the expressions for the success probability of packet delivery and its components, such as the header and payload reception probabilities. The simulation model implements a Monte Carlo approach to validate the analytical results and account for the effects of satellite mobility, Rician fading, and capture effect. The findings demonstrate that LR-FHSS can effectively support large-scale networks of infrequently reporting devices in remote areas. The results also reveal trade-offs between the two data rates defined for the EU region, indicating that the choice of data rate can significantly impact the network performance. Furthermore, the results identify the loss of headers as the primary reason for packet loss, suggesting that improving header reception can greatly enhance the overall packet delivery probability. These results provide valuable insights into the performance and potential of LR-FHSS for satellite IoT and pave the way for future research in this area.

Additionally, investigations like (ÁLVAREZ *et al.*, 2022) leverage innovative approaches, such as exploiting satellite trajectory, further augmenting the gains observed with LR-FHSS. The authors propose a beacon-based system model that builds on LoRa and LR-FHSS modulations. This model introduces multiple Direct-to-Satellite Internet of Things (DtS-IoT) specific uplink transmission policies that leverage the available information of the satellite trajectory. The results of the simulation showed that the proposed Trajectory-based approaches outperformed the baseline approaches. Specifically, the conservative or random selection of Spreading Factors and Data Rates in LoRa and LR-FHSS, respectively, were surpassed by the new model. The use of trajectory information was found to at least double the network scalability compared to non-trajectory aware schemes. Furthermore, skip-based trajectory uplink transmission policies provided a 30% boost when the network approached saturation.

The article by (MALEKI *et al.*, 2023b) presents an analytical approach for deriving the outage probability of LR-FHSS in a satellite-based IoT network. The authors consider the effects of noise, channel fading, path loss, and capture effect on the performance of LR-FHSS. The article provides closed-form expressions for the outage probability and validates them with computer simulations. The results show that LR-FHSS can achieve significant capacity improvement compared to the conventional LoRa modulation, especially for high-density scenarios.

The studies conducted in (JUNG *et al.*, 2023) outline a pioneering effort to develop a novel transceiver design tailored specifically for DtS-IoT systems utilizing LR-FHSS modulation. With a primary focus on enhancing LR-FHSS performance in satellite communication environments, the research addresses critical challenges such as the Doppler effect and the reception of multiple frequency-hopping signals. By proposing modifications to both transmitter and receiver structures, including refined preamble insertion and robust signal detection mechanisms, the study aims to optimize LR-FHSS-based communication for DtS-IoT systems. Through comprehensive simulations conducted in realistic Low Earth Orbit (LEO) satellite channel environments, the proposed transceiver design demonstrates superior performance metrics compared to benchmark schemes, highlighting its potential to enhance reliability and efficiency in satellite-based IoT communications.

The research conducted in (ZHANG *et al.*, 2023) reveals that within the same set of sub-channels, the selection of different Frequency Hopping Sequences (FHS) can lead to a substantial variation in reliability, with Packet Reception Rate (PRR) differing by up to 52.6%. To address this challenge, the paper introduces Dynamic Frequency Hopping (DFH), a novel method that integrates both link quality and FHS considerations to enhance LR-FHSS transmission reliability in dynamic environments. The proposed approach utilizes hop Signal-to-Noise Ratio (SNR) as a refined metric to characterize sub-channel conditions. It establishes a predictive model for Packet Reception Rate (PRR) based on hop SNR and FHS. Through careful parameter selection and the implementation of an interleaving-based search algorithm, DFH efficiently identifies optimal FHS configurations, improving PRR by up to 2.76 times compared to standard LR-FHSS methods.

To amplify the decoding performance in scenarios with increased concurrent signal reception over the same hopping bandwidth, the authors of (TEMIM *et al.*, 2023) introduce several interference blanking techniques. Through experimentation, the authors demonstrate significant decoding improvements, highlighting that their interference blanking methods enable the decoding of 250 LR-FHSS signals within 5 seconds using a hopping bandwidth of 183.488 kHz with a Packet Error Rate (PER) of 10^{-2}, compared to the receiver's limitation of decoding 100 signals without interference processing. This enhancement holds promise for substantially augmenting the uplink capacity of LoRaWAN-based networks, as LR-FHSS exhibits superior throughput over conventional LoRa PHY layers, as previously demonstrated.

Furthermore, it is widely acknowledged in coding theory that despite their simplicity, repetition codes are not optimal for error correction (LIN; COSTELLO, 2004). This observation extends to the cooperative communication concept, as demonstrated by studies such as that by (XIAO; SKOGLUND, 2010; REBELATTO *et al.*, 2012). These studies show that MDS-based network codes can notably enhance diversity order, thus improving reliability compared to simpler repetition codes. This underscores the significance of employing more advanced coding techniques, particularly in cooperative communication contexts, to maximize error correction capabilities and enhance overall system performance.

The study by (ALVES *et al.*, 2022) investigates the outage probability in LoRa networks by applying network-coded techniques. The paper introduces NCC-LoRa, a scheme facilitating EDs to communicate through Device to Device (D2D) and transmit linear combinations of multiple frames to a shared Gateway (GW). Within their analysis, the authors integrate connection and collision probabilities into the outage probability model for EDs, alongside a realistic power consumption model. Their findings illustrate significant enhancements in outage probability with Network-Coded Cooperation Long Range (NCC-LoRa), potentially consuming less energy than traditional LoRa and RT-LoRa, even with the inclusion of D2D communication.

The study conducted by (MALEKI *et al.*, 2023a) introduces a cooperative network coding approach employing D2D communication and LR-FHSS to enhance the reliability and scalability of DtS-IoT networks. They derive a closed-form expression for the outage probability of the LR-FHSS scheme within a shadowed-Rice channel model. The authors meticulously analyze the outage probabilities of both LR-FHSS and D2D-aided LR-FHSS schemes, considering practical channel characteristics such as shadowed-Rice fading, interference, and capture effect. The research outlines the channel models and system parameters for uplink and downlink transmissions and derives expressions for the outage probability, average bit error rate, and spectral efficiency. Furthermore, the authors investigate the impact of satellite movements and ED locations on outage probability and propose an effective time-scheduling algorithm for future research. The study underscores the challenges and opportunities in this domain, demonstrating significant enhancements of D2D-aided LR-FHSS over LR-FHSS in terms of network capacity and outage performance across various data rates and network densities. This underscores the potential of the proposed D2D-aided LR-FHSS scheme for future DtS-IoT applications.

3 PRELIMINARIES

This chapter provides a comprehensive examination of LR-FHSS, elucidating this technology, its computational aspects, and its practical applications. Initially, we present the fundamentals of LoRa and LR-FHSS, emphasizing their modulation distinctions. The essence of this paper is a detailed exposition of critical calculations such as ToA, outage probability, and error probability in LR-FHSS networks. Subsequently, we detail the process of constructing a collision model based on transmitted packet times and channel checks for overlaps. Lastly, we discuss the application of network coding techniques in LR-FHSS headers.

3.1 LoRa MODULATION

LoRa is a modulation technique developed and patented by the company Semtech Corporation (SELLER, 2017), representing a breakthrough in wireless communication, particularly for scenarios where energy-efficient, long-range connectivity is of paramount importance. Unlike traditional modulation schemes that rely on fixed carrier frequencies, LoRa employs CSS modulation. This modulation technique involves continuously varying the carrier frequency over time to convey information. In this thesis, we explore the intricacies of LoRa modulation, providing insights into its fundamental principles and practical applications.

In CSS modulation, a binary '1' corresponds to an upward chirp, characterized by a gradually increasing frequency over time. On the other hand, a binary '0' is conveyed by a downward chirp, featuring a decreasing frequency trend. This approach enables the transmission of binary data within the chirp signal, and effectively reduces the impact of noise in wireless channels, making it a suitable choice for applications requiring long-range network coverage and low energy consumption (SUNDARAM *et al.*, 2020). The modulation parameters of LoRa that determine the timing of each packet include: the transmission bandwidth $B \in 125, 250, 500$ kHz, the SF, $\mathcal{S}_{\rm F} \in 7, \ldots, 12$, and the CR, CR $\in 1, \ldots, 4$.

Bandwidth refers to the width of the spectrum used for transmitting data. Smaller bandwidths result in longer communication ranges but lower data rates, while larger bandwidths offer higher data rates but shorter ranges. The choice of bandwidth impacts both the range and the speed of communication. Common LoRa bandwidths include 125 kHz, 250 kHz, and 500 kHz.

Table 1 – LoRa characteristics for CR = 1 and $B = 125$ kHz, 9 byte payload with CRC and low data rate optimization enabled, and implicit header mode disabled.

SF $\mathcal{S}_\text{F}$	**Time-on-Air** ToA (ms)	**Bit Rate** R_b (kbps)	**Receiver Sensitivity** S (dBm)
7	41.22	5.47	−123
8	72.19	3.13	−126
9	144.38	1.76	−129
10	247.81	0.98	−132
11	495.62	0.54	−134.5
12	991.23	0.29	−137

The spreading factor determines how much the signal is spread out in time and frequency. LoRa offers different spreading factors, with higher values (e.g., SF12) providing better range and lower data rates, while lower values (e.g., SF7) offer higher data rates at the cost of reduced range. Coding rate refers to the amount of error correction coding applied to the transmitted data. Higher coding rates (e.g., 2/3) provide better error correction but reduce available bandwidth and data rate. Lower coding rates (e.g., 1/3) offer higher data rates but with less error correction. The aforementioned factors are used to calculate the ToA (in seconds) as (SEMTECH CORPORATION, 2019):

$$\text{ToA}_\text{LoRa} = \frac{2^{\mathcal{S}_\text{F}}}{B}\left(n_\text{pre} + n_\text{pay} + 4.25\right), \tag{1}$$

where n_pre and n_pay are respectively the number of LoRa preamble and payload symbols, being the last obtained as (SEMTECH CORPORATION, 2019)

$$n_\text{pay} = 8 + \max\left\{0, (\text{CR} + 4)\left\lceil \frac{44 + 8\text{PL} - 4\mathcal{S}_\text{F}}{4\left(\mathcal{S}_\text{F} - 2\text{DE}\left(\mathcal{S}_\text{F}\right)\right)}\right\rceil\right\}, \tag{2}$$

where $\mathcal{S}_\text{F}$ is the spreading factor, CR the code rate and PL the payload length (in bytes). In (2), $\text{DE}\left(\mathcal{S}_\text{F}\right)$ represents a low rate optimization function that assumes respectively values 1 or 0 for $\mathcal{S}_\text{F} \geq 11$ and $\mathcal{S}_\text{F} < 11$. Finally, the transmission rate R_b (in bits/s) is calculated as (SEMTECH CORPORATION, 2019):

$$R_b = \mathcal{S}_\text{F} B \frac{2^{2-\mathcal{S}_\text{F}}}{(4 + \text{CR})} \quad \text{[bits/s]}. \tag{3}$$

As can be shown from (1), the ToA increases exponentially with the SF, reducing the effective transmission rate. In turn, the receiver sensitivity S and the minimum reception SNR Ψ increase with the SF. The values of S and Ψ according to the technical documentation of the LoRa-based Semtech SX1272 device (SEMTECH CORPORATION, 2019) are presented in Table 1.

LoRaWAN is a communication protocol established by the LoRa Alliance, defining a network architecture over the LoRa physical layer. In this protocol, ED communicate exclusively with a GW in a star topology. The GW then forwards data from the EDs to the Network Server (NS) via an IP link. While LoRaWAN is commonly used for LoRa networks, it is important to note that LoRa networks may not necessarily utilize LoRaWAN, as LoRa operates independently of higher communication protocol layers.

3.2 LR-FHSS

LR-FHSS, introduced by LoRa Alliance in the RP2-1.0.2 LoRaWAN specification (LORA ALLIANCE, INC., 2021), represents a fast FHSS modulation designed specifically for the uplink of LoRaWAN networks. In this approach, the frequency range is partitioned into multiple Occupied Channel Width (OCW) channels, with their bandwidths subject to regional regulations (LORA ALLIANCE, INC., 2021). These OCW channels are further subdivided into several physical frequency channels, known as Occupied Bandwidth (OBW) channels, each having a bandwidth of 488Hz. Consequently, at any given moment, an ED transmits in a single OBW channel, adhering to a predetermined frequency hopping pattern determined by a Pseudo-Random Number Generator (PRGN)(BOQUET *et al.*, 2021). The spread spectrum fragment along the channel enhances the resilience and robustness of the network against interference while optimizing spectral efficiency, thus facilitating reliable and efficient communication within LoRaWAN deployments.

In countries following the ETSI standards, LR-FHSS channels are separated by a minimum of 3.9 kHz (grid), and the frequency hopping bandwidth is 137 kHz. This configuration provides a total of 280 available physical channels (8×35). Channel changes, or hops, occur every $T_{\mathrm{H}} = 233.472$ ms for headers and every $T_{\mathrm{frag}} = 102.4$ ms for payload fragments. The transmission process begins by selecting a random channel, followed by announcing the random frequency hopping pattern through the packet header. This mechanism ensures equal statistical utilization of all channels, facilitating efficient communication within the network.

The ToA varies according the selected DR as (LORA ALLIANCE, INC., 2021)

$$\mathrm{ToA}_{\mathrm{LR}} = N_{\mathrm{H}}\, T_{\mathrm{H}} + T_{\mathrm{frag}} \left\lceil \frac{\mathrm{PL} + 3}{6R} \right\rceil, \tag{4}$$

where PL is the number of payload bytes and R is the payload error correcting code rate, which is $R = 1/3$ for DR8 and $R = 2/3$ for DR9. Moreover, N_{H} is the number of transmitted PHY header replicas, being $N_{\mathrm{H}} = 3$ for DR8 and $N_{\mathrm{H}} = 2$ for DR9. Table 2 summarizes the LR-FHSS DR8/DR9 parameters (LORA ALLIANCE, INC., 2021).

Table 2 – LR-FHSS main specifications and parameters for the European Union (ETSI, 863-870 MHz) (LORA ALLIANCE, INC., 2021).

		DR8	**DR9**
LR-FHSS number of channels		8	
Carriers for FH per ED		35	
Carriers for FH per OCW channel	C	280 (8x35)	
Coding rate	R	$1/3$	$2/3$
Number of header replicas	N_{H}	3	2
Duration of each header replica [s]	T_{H}	0.2334	
Duration of each payload fragment [s]	T_{frag}	0.1024	
Payload length	PL	10	
Payload duration [s]	T_{L}	$T_{\mathrm{frag}}\left\lceil\frac{\mathrm{PL}+3}{2}\right\rceil$	$T_{\mathrm{frag}}\left\lceil\frac{\mathrm{PL}+3}{4}\right\rceil$
Number of payload fragments	N_{L}	$\lceil T_{\mathrm{L}}/T_{\mathrm{frag}}\rceil$	
Duration of a packet (time-on-air) [s]	$\mathrm{ToA}_{\mathrm{LR}}$	$N_{\mathrm{H}}T_{\mathrm{H}}+T_{\mathrm{L}}$	
Maximum duty cycle	ρ	0.01 (1%)	
Average packets/hour/device	$\mathcal{P}_{\mathrm{hour}}$	$3600\rho/\mathrm{ToA}$	

Moreover, it is worth noting that within the LR-FHSS scope, Data Rate (DR) primarily delineates the error-correcting code rate and the number of header replicas, whereas in the standard LoRa scheme presented in Section 3.1, each DR corresponds to a distinct spreading factor.

3.2.1 Analytical Performance of LR-FHSS

In this section, we will describe the analytical model developed in (ULLAH *et al.*, 2022a) to evaluate the performance of LR-FHSS networks. More specifically, we focused on the packet success probability and its complement, the so-called packet error probability.

For that sake, let μ represent the average inter-arrival time of packet elements. This inter-arrival time depends on the number of nodes $\mathcal{N}$ and the average number of packets per hour per device $\mathcal{P}_{\mathrm{hour}}$. Specifically, $\mu_i = 3600/(\mathcal{N}\,\mathcal{P}_{\mathrm{hour}}\,N_i)$, where $i \in \{\mathrm{H,L}\}$, with H referring to headers and L to payloads. Moreover, N_{H} is the number of header replicas, and N_{L} is the number of payload fragments.

Let us assume that each packet element is subject to an erasure probability, denoted by ϵ, which is considered to be independent and identically distributed (i.i.d.) across time, frequency, or space. This erasure probability model, extensively employed in ALOHA scheme analyses (MUNARI *et al.*, 2021; KASSAB *et al.*, 2020), strikes a balance between mathematical feasibility and the modeling of fading and shadowing losses. It is essential to note that the specific value of ϵ depends on multiple factors such as device-to-satellite distance, carrier frequency, antenna gains, data rate, noise figure, and random blockages, among others. Determining the erasure probability involves assessing the outage probability considering the aforementioned aspects, a complex task beyond the scope of this work. The objective of this work lies in demonstrating the advantages derived from appropriately combining header replicas as opposed to simple replication, thereby augmenting reliability or enabling support for a larger number of devices. Nevertheless, we present in Appendix A some additional analysis to support the erasure channel model adopted in this work.

The average number of packet elements arriving at the gateway during header and payload transmissions can be calculated as follows (ULLAH *et al.*, 2022a):

For headers:

$$A_{\mathrm{H}} = \left[\frac{1}{\mu_{\mathrm{H}}}\left(2T_{\mathrm{H}}\right) + \frac{1}{\mu_{\mathrm{L}}}\left(T_{\mathrm{H}} + T_{\mathrm{frag}}\right)\right](1-\epsilon). \tag{5}$$

For payloads:

$$A_{\mathrm{L}} = \left[\frac{1}{\mu_{\mathrm{L}}}\left(2T_{\mathrm{frag}}\right) + \frac{1}{\mu_{\mathrm{H}}}\left(T_{\mathrm{H}} + T_{\mathrm{frag}}\right)\right](1-\epsilon). \tag{6}$$

The probability of successfully receiving an individual packet element either of a header or payload can be calculated as (ULLAH *et al.*, 2022a):

$$p_i = \left(1 - \frac{1}{C}\right)^{A_i - 1}(1-\epsilon) \tag{7}$$

where C represents the number of channels within an OCW channel for frequency hopping.

Successful packet reception at the destination relies on the simultaneous occurrence of two independent events, as detailed in (ULLAH *et al.*, 2022a). The first event involves the reception of at least one out of the N_{H} transmitted header replicas, whose probability of occurrence is:

$$P_{\mathrm{H}} = 1 - \left(1 - p_{\mathrm{H}}\right)^{N_{\mathrm{H}}}. \tag{8}$$

The second event focuses on payload fragment reception, calculating the probability of successfully receiving at least $(R\,N_{\mathrm{L}})$ payload fragments out of the total transmitted N_{L} transmitted fragments. The probability of such an event can be calculated as (ULLAH *et al.*, 2022a)

$$P_{\mathrm{L}} = \sum_{n=ceil(R\,N_{\mathrm{L}})}^{N_{\mathrm{L}}} \binom{N_{\mathrm{L}}}{n} p_{\mathrm{L}}^{n}(1-p_{\mathrm{L}})^{N_{\mathrm{L}}-n}. \tag{9}$$

These established criteria serve as fundamental benchmarks for determining successful packet reception, accounting for both header and payload components, vital in assessing the reliability of data transmission systems.

A packet is considered successfully received at the destination when both events (related to header and payload) are concurrently met. Thus, the overall success probability can be calculated as:

$$p_{\text{success}} = P_{\text{H}}\, P_{\text{L}}, \tag{10}$$

where P_{H} and P_{L} are the probabilities of successfully receiving headers and payloads from (8) and (9), respectively.

The Packet Error Probability (PEP) is complementary to the success probability expressed in (10):

$$p_{\text{error}} = 1 - p_{\text{success}}. \tag{11}$$

3.2.2 LR-FHSS Simulator

In this section, we present the MATLAB®-based LR-FHSS simulator developed in (ULLAH *et al.*, 2022a) and available on GitHub (ULLAH *et al.*, 2022b). The simulator's purpose is to analyze network performance by generating random timestamps for packet transmissions, calculating collisions during header and payload transmissions, and determining successful receptions.

As illustrated in the flowchart presented in Fig 1, the simulator can be divided into three main parts, which are explained below.

1. **Timestamp generation:** The timestamp for each packet transmission is randomly generated, which represents the start time of each packet transmission within a one-hour interval.

2. **Fragment collision detection:** The collisions that occur during the transmission of header replicas and payload fragments are detected. A collision happens when more than one packet element starts transmitting, in the same channel, within the time window $[t - \text{ToA}, t + \text{ToA}]$, where ToA is the Time on Air calculated using (4).

3. **Evaluate the received fragments:** Determining whether a packet is successfully received or not, by evaluating the number of header replicas and payload fragments received. More specifically, the packet is correctly recovered when:

    - At least one out of the N_{H} header replicas is received without collision.
    - At least $R\, N_{\text{L}}$ out of the N_{L} payload fragments are correctly received.

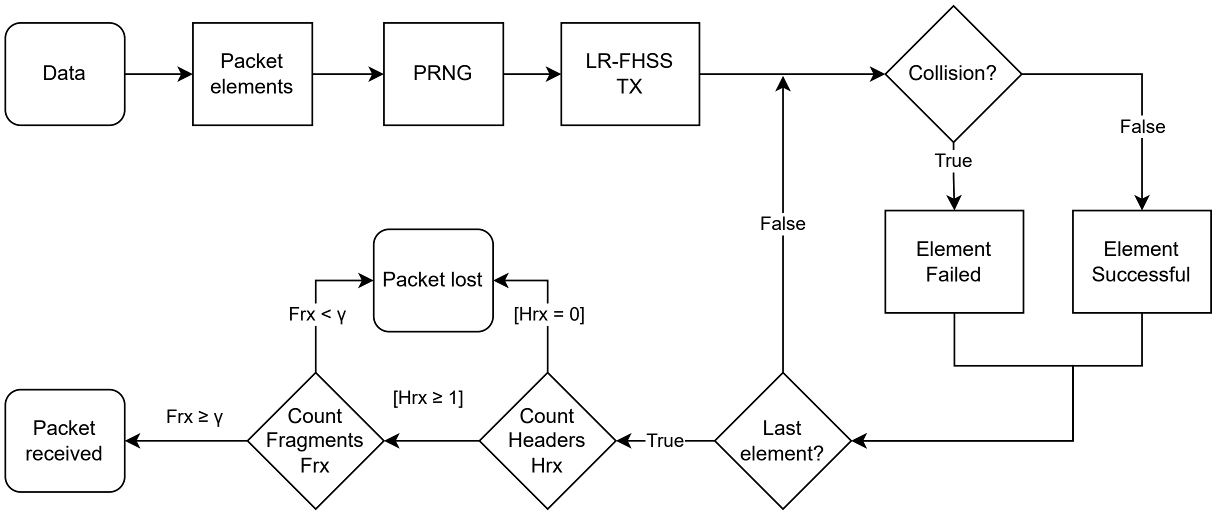

Figure 1 – LR-FHSS simulator flowchart, adapted from (ULLAH *et al.*, 2022a).

3.2.3 Error Probability of LR-FHSS

This subsection aims at illustrating the error probability of LR-FHSS by comparing the results obtained using the analytical model from Section 3.2.1 and the simulator presented in Section 3.2.2.

To that end, we present in Fig. 2 the error probability as a function of the number of end devices for a LR-FHSS network operating under DR8 and with PL $= 10$ bytes. The markers refer to the simulation results, while the lines correspond to the analytical values. Specifically, the following results are presented in Fig 2:

- **Overall** error probability, whose analytical value is obtained from (11) and represented by the full red line (—).
- **Header** error probability, whose analytical value is obtained from the complement of (8) and represented by the dotted red line (· · ·).
- **Payload** error probability, whose analytical value is obtained from the complement of (9) and represented by the dash-dot red line (—·).

First, one can see that the simulation results support the analytical model with good accuracy. The small difference noticed for small values of error probability comes from the number of Monte Carlo trials in the simulations. That is, one should have simulated the transmission of a larger number of packets to reach such a small average error probability.

Moreover, it is noteworthy from Fig. 2 that, as highlighted in (ULLAH *et al.*, 2022a), the overall error performance of the LR-FHSS scheme is heavily influenced by the header

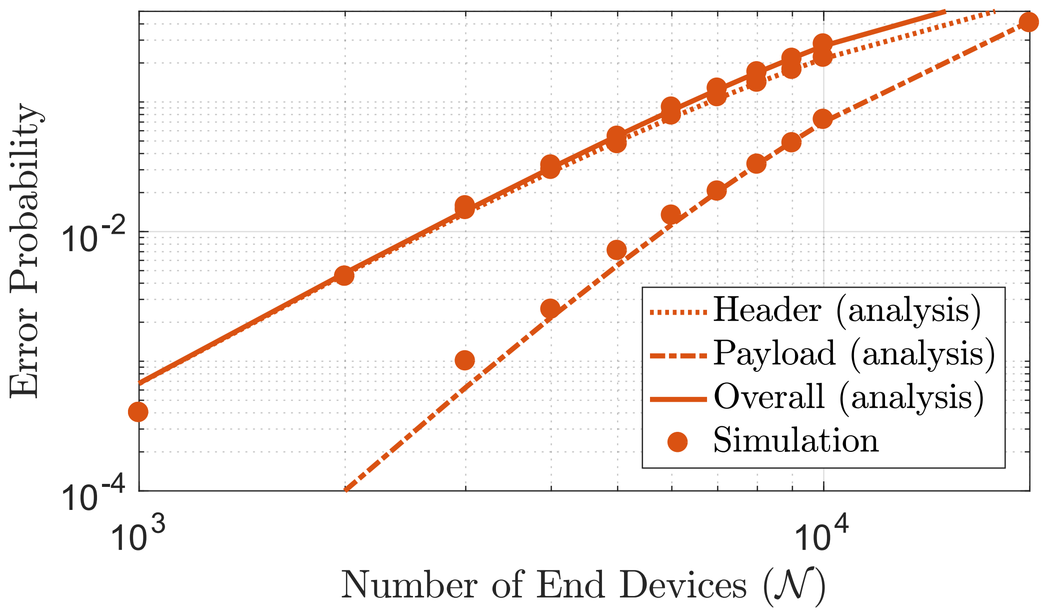

Figure 2 – Error probability of header, payload, and overall packet as a function of the number of end-devices $\mathcal{N}$, considering DR8 and PL $= 10$ bytes.

error probability. That is, the repetition coding scheme adopted to protect the headers against errors/collisions does not present the same reliability as the payload fragments, which somewhat compromises the LR-FHSS overall performance. Notably, headers are more than twice as long as the payload, which makes them more prone to collisions.

4 PROPOSED LR-FHSS-NC SCHEME

This chapter introduces and evaluates the performance of the proposed LR-FHSS-NC scheme. The proposed scheme resorts to classical error correcting coding theory to boost the reliability of the headers at the cost of an increased delay, but without compromising throughput (does not increase the bandwidth) nor requiring additional transmit power.

The idea behind LR-FHSS-NC is to properly combine the headers of multiple packets from the same ED before the transmission of their associated payload fragments. Such an idea comes from the cooperative communication setup from (XIAO; SKOGLUND, 2010; REBELATTO *et al.*, 2012), where the authors showed that gains in reliability can be achieved by properly combining multiple packets before transmission, as opposed to sending them separately, which does happen in the standard LR-FHSS header replicas.

According to (REBELATTO *et al.*, 2012), the term "properly combining" can be translated to a technical field as combining the packets by *adopting as coefficients of the combinations the symbols from a generator matrix of a linear Error Correcting Code (ECC) with the maximum possible minimum distance* d_{min}. The minimum distance of an ECC is the minimum Hamming distance between two different codewords, being a fundamental parameter of code design that determines the maximum number of errors that can be corrected by the code (LIN; COSTELLO, 2004).

Let us consider an ECC with parameters (n,k,d_{min}) and code rate k/n. Thus, one has that the minimum distance is upper bounded by the so-called Singleton bound as (LIN; COSTELLO, 2004):

$$d_{\text{min}} \leq n - k + 1. \tag{12}$$

A code that achieves the maximum possible minimum distance ($d_{\text{min}} = n - k + 1$) in (12) is said to be a MDS code. The RS is a widespread class of MDS codes, being defined over a nonbinary field GF(q), where q represents the field size. The higher the code dimensions (*i.e.*, the values of n and k), the higher the field size q necessary for the code to be MDS.

Bringing such classical theory to the LR-FHSS scope, let us consider $N_{\text{H}} = 3$ for DR8, and refer to H_1 as the header of a given packet numbered, without loss of generality, as packet 1. Thus, since the same header is replicated N_{H} times, one can see this replication scheme as a linear (block) ECC of rate $1/N_{\mathsf{H}}$ and whose coding process is performance as presented below[1]

$$\begin{bmatrix}H_1\end{bmatrix} \times \begin{bmatrix}1 & 1 & 1\end{bmatrix} = \begin{bmatrix}H_1 & H_1 & H_1\end{bmatrix},$$

where $\begin{bmatrix}1 & 1 & 1\end{bmatrix}$ is the generator matrix $\mathbf{H}$ of a $1/3$-rate ECC with parameters $(n = 3, k = 1)$, such that the minimum distance is upper bounded by $d_{\text{min}} \leq n - k + 1 = 3$. When operating under such code, H_1 is correctly received at the GW when at least one out of the 3 replicas are correctly received. In other words, the code can properly handle 2 ($N_{\mathsf{H}} - 1$, in general) replica losses.

Now, let us elaborate and consider a scenario where, before the transmission of packet 1, the same ED accumulates an amount of δ packets, which, for illustrative purposes, we particularize to $\delta = 2$ and refer to the second packet as packet 2, whose header is H_2. Then, such an ED could first transmit both H_1 and H_2 before the transmission of the payload fragments of both packets. Still considering $N_{\mathsf{H}} = 3$ for DR8, one possibility would be to adopt the following coding approach:

$$\begin{bmatrix}H_1 & H_2\end{bmatrix} \times \underbrace{\begin{bmatrix}1 & 1 & 1 & 0 & 0 & 0\\ 0 & 0 & 0 & 1 & 1 & 1\end{bmatrix}}_{\text{Generator matrix } \mathbf{H}} = \begin{bmatrix}H_1 & H_1 & H_1 & H_2 & H_2 & H_2\end{bmatrix}. \tag{13}$$

In this new scenario, even though the ECC characterized by $\mathbf{H}$ still has the code rate $2/6 = 1/3$, its dimensions are increased to $(n = \delta N_{\mathsf{H}} = 6, k = \delta = 2)$, such that the minimum distance is now upper bounded by $d_{\text{min}} \leq 6 - 2 + 1 = 5$. However, although there exists an error event in which the aforementioned code is capable of handling four errors and still recovers both H_1 and H_2, there also exists an error event when only three errors make either H_1 or H_2 to be unrecoverable by the GW. Such events are illustrated in what follows, where a crossed symbol represents a lost header replica at the GW side.

$$\begin{bmatrix}\cancel{H_1} & \cancel{H_1} & H_1 & \cancel{H_2} & \cancel{H_2} & H_2\end{bmatrix} \rightarrow \text{4 errors and both } H_1 \text{ and } H_2 \text{ are recovered.}$$

$$\begin{bmatrix}\cancel{H_1} & \cancel{H_1} & \cancel{H_1} & H_2 & H_2 & H_2\end{bmatrix} \rightarrow \text{Only 3 errors and } H_1 \text{ is lost.}$$

Thus, it becomes clear that although increasing the code size increases the **achievable** minimum distance, the repetition code presented above fails in increasing the header reliability,

[1] Note that the frequency axis and the frequency hopping characteristic of LR-FHSS are intentionally omitted in the example aiming at easing the understanding. In practice, each replica would be transmitted in a different frequency channel.

since there exists an event with N_{H} header errors that cause a packet loss, exactly as in the standard LR-FHSS case.

4.1 LR-FHSS-NC AND THE LINEAR COEFFICIENTS DESIGN

Thus, as discussed in the previous section, the repetition code approach fails in providing the maximum protection achievable by the an ECC with rate $\delta/(\delta N_{\mathsf{H}})$, whose minimum distance is upper bounded as $d_{\text{min}} \leq \delta(N_{\mathsf{H}} - 1) + 1$ (this is obtained by substituting $k = \delta$ and $n = \delta N_{\mathsf{H}}$ in the Singleton bound from (12)). Our proposal is then to perform linear combinations between the δ header replicas by adopting as coefficients the symbols of the generator matrix an MDS ECC. Although there exist several classes of MDS codes, we follow (REBELATTO *et al.*, 2012) and pick the linear coefficients from the generator matrix of the Reed-Solomon codes (REED; SOLOMON, 1960), a class of non-binary linear block codes.

In the scenario with $N_{\mathsf{H}} = 3$ and $\delta = 2$ presented in the previous section, one would have that the linear combinations between H_1 and H_2 when operating under LR-FHSS-NC are

$$\begin{bmatrix} H_1 & H_2 \end{bmatrix} \times \underbrace{\begin{bmatrix} 1 & 0 & 3 & 1 & 5 & 7 \\ 0 & 1 & 2 & 3 & 4 & 6 \end{bmatrix}}_{\text{Generator matrix } \mathbf{H}} = \begin{bmatrix} H_1 \\ H_2 \\ 3H_1 \boxplus 2H_2 \\ H_1 \boxplus 3H_2 \\ 5H_1 \boxplus 4H_2 \\ 7H_1 \boxplus 6H_2 \end{bmatrix}^T, \tag{14}$$

where $[\cdot]^T$ is the transpose operation and $\boxplus$ represents the summation over a nonbinary finite field. In this example, the RS code is defined over a finite field GF(8), such that all the operations (summation, etc) performed over such field must result in a symbol $\{0, \ldots, 7\}$ within the field. For more details about operations over a finite field we refer the reader to Appendix B. As a result, instead of transmitting the headers of the δ packets individually, as illustrated in (13), one would transmit such δN_{H} replicas in a coded fashion, following (14). This transmission protocol is illustrated in Fig. 3, when also the frequency dimension is taken into account. Note that LR-FHSS-NC does not demand additional time on air to transmit the coded replicas. In fact, the δ packets still demand an overall time-on-air of δToA.

In the example from (13), we concluded that there exists an event of three errors that leads to a lost header (and consequently to a lost packet) at the GW. Now, when adopting the

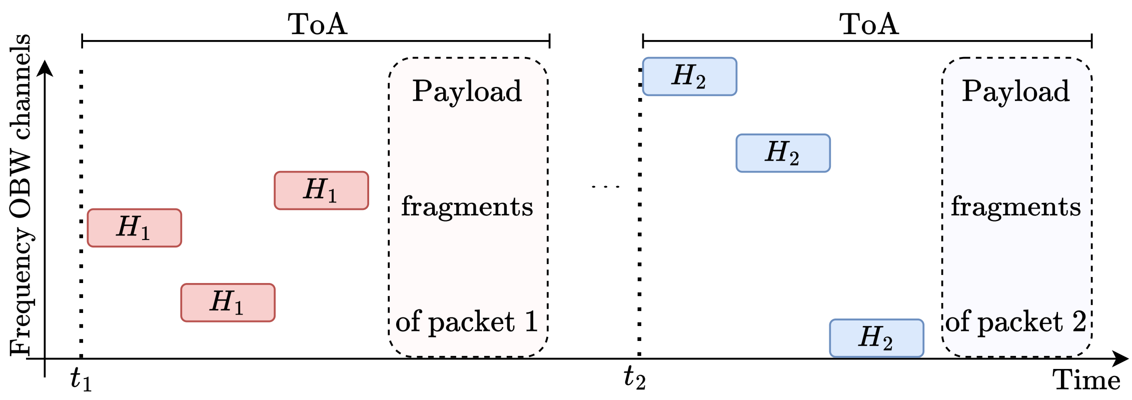

(a) LR-FHSS (DR8 with $N_H = 3$).

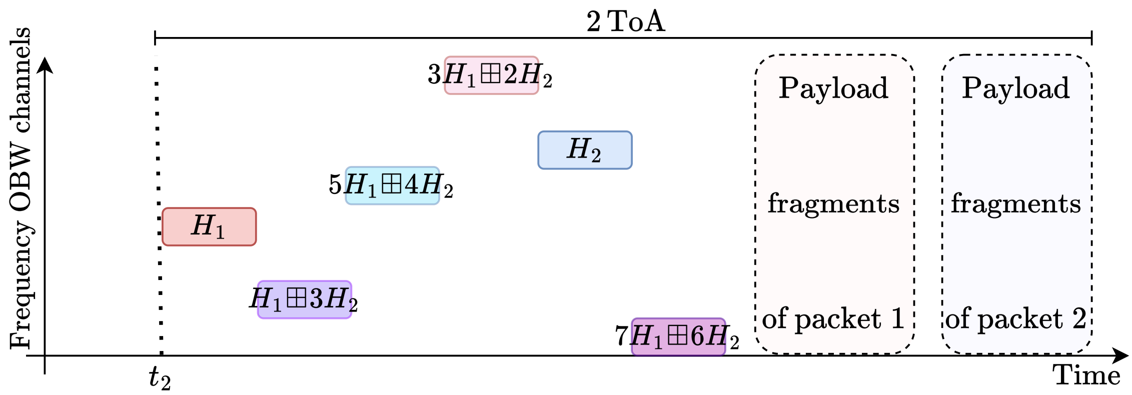

(b) LR-FHSS-NC ($N_H = 3$ and $\delta = 2$).

Figure 3 – Example of LR-FHSS-NC: The header replicas of $\delta = 2$ packets are linearly combined in (b). The average packet time-on-air remains the same as in the standard LR-FHSS, as depicted in (a).

MDS-based combinations from (14), all the coded replicas are linearly independent (this is a characteristic of an MDS code), such that both H_1 and H_2 can be recovered from any 2 out of the 6 transmitted replicas.

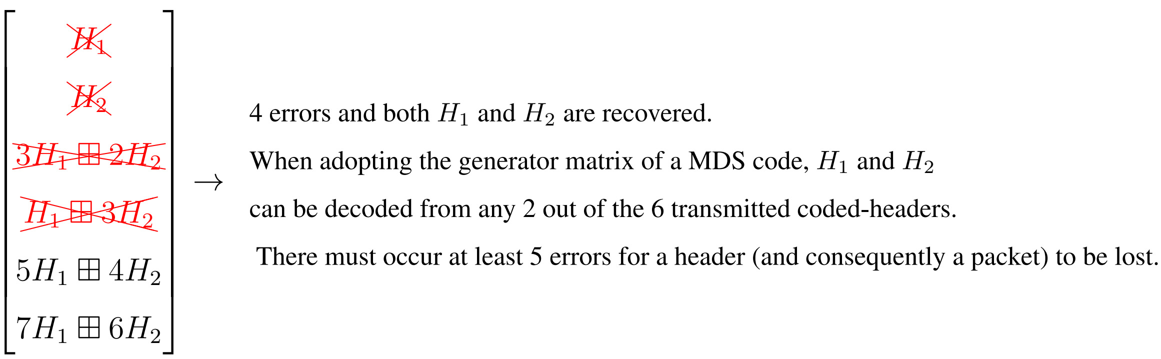

In this example, upon receiving the coded-headers $5H_1 \boxplus 4H_2$ and $7H_1 \boxplus 6H_2$, the GW can extract the headers H_1 and H_2 by solving the correspondent linear system through Gaussian Elimination, for example.

The elements of the transmitted packet for both the regular LR-FHSS and the proposed

Table 3 – Transmitted packet elements for the regular LR-FHSS and the proposed LR-FHSS-NC scheme with $\delta = 2$.

Scheme	**# Replicas**							Transmitted replicas		**Diversity**
	N_H	Total of $\delta \times N_\mathsf{H}$ replicas								$(N_\mathsf{H}-1)L+1$
LR-FHSS	2	H_1	H_1	(payload 1)	H_2	H_2	(payload 2)			2
LR-FHSS	3	H_1	H_1	H_1	(payload 1)	H_2	H_2	H_2	(payload 2)	3
LR-FHSS-NC	2	H_1	H_2	$H_1 \boxplus H_2$	$H_1 \boxplus 2H_2$	(payload 1)	(payload 2)			3
LR-FHSS-NC	3	H_1	H_2	$3H_1 \boxplus 2H_2$	$5H_1 \boxplus 4H_2$	$H_1 \boxplus 3H_2$	$7H_1 \boxplus 6H_2$	(payload 1)	(payload 2)	5

LR-FHSS-NC scheme with $\delta = 2$ are listed in Table 3, considering both DR8 ($N_\mathsf{H} = 3$) and DR9 ($N_\mathsf{H} = 2$). It is also worth mentioning that the devices do not necessarily need to store a large number of different matrices, since different scenarios (namely, different values of N_H and δ) can be encompassed by adopting elementary coding operations such as *puncturing* (LIN; COSTELLO, 2004; REBELATTO *et al.*, 2012).

The key advantage of LR-FHSS-NC lies in its ability to enhance header reliability by transmitting each header with a larger number of replicas, all while maintaining a consistent number of transmitted replicas per packet. This approach substantially improves the likelihood of successful header reception, contributing to increased overall network reliability and reduced packet error rates, as long as the replicas are subjected to independent erasures and collisions.

4.2 SUCCESS PROBABILITY OF THE LR-FHSS-NC SCHEME

In this section, we delve into the mathematical foundations of calculating the success probability for the LR-FHSS-NC scheme. As discussed earlier, LR-FHSS-NC aims to enhance the reliability of header reception while preserving the payload transmission characteristics of regular LR-FHSS. Thus, the payload success probability remains the same as presented in (9). However, the probability $P_\mathsf{H}\,(N_\mathsf{H},\delta)$ of correctly receiving a header in the LR-FHSS-NC scheme with parameters N_H and δ is now given by

$$P_\mathsf{H}(N_\mathsf{H},\delta) = \sum_{n=\delta}^{\delta N_\mathsf{H}} \binom{\delta N_\mathsf{H}}{n} p_\mathsf{H}^n (1 - p_\mathsf{H})^{\delta N_\mathsf{H} - n}, \tag{15}$$

where p_H represents the individual probability of successfully receiving a coded-replica, as described by (7) and $\binom{a}{b}$ denotes the binomial coefficient.

In LR-FHSS-NC, assuming the coefficients of the linear combinations are chosen in a way that ensures linear independence (typically achieved through the use of a MDS code), the system involves δN_H equations and δ variables. The success criterion for this system is set to correctly receive at least δ out of the δN_H coded-replicas. Each coded-replica can be successfully received with a probability represented by $\binom{\delta N_\mathsf{H}}{n} p_\mathsf{H}^n (1 - p_\mathsf{H})^{\delta N_\mathsf{H} - n}$. The probability expressed in (15) is obtained by considering all the events within the range $\delta \leq n \leq \delta N_{\mathsf{H}}$ and summing their respective probabilities.

Finally, the overall success probability for the LR-FHSS-NC scheme, encompassing both header and payload reception, is determined by incorporating the success probability from (15) into the general success probability formula given by (10), which leads to

$$p_{\text{success}}^{\text{NC}} = \underbrace{\left[\sum_{n=\delta}^{\delta N_{\mathsf{H}}} \binom{\delta N_{\mathsf{H}}}{n} p_{\mathsf{H}}^{n} (1 - p_{\mathsf{H}})^{\delta N_{\mathsf{H}} - n}\right]}_{\text{Header success probability from (15)}} \overbrace{\left[\sum_{n=R\,N_{\text{L}}}^{N_{\text{L}}} \binom{N_{\text{L}}}{n} p_{\text{L}}^{n} (1 - p_{\text{L}})^{N_{\text{L}} - n}\right]}^{\text{Payload success probability from (9)}}. \tag{16}$$

The error probability is obtained from the complement of (16) as

$$p_{\text{error}}^{\text{NC}} = 1 - p_{\text{success}}^{\text{NC}}. \tag{17}$$

4.3 LR-FHSS-NC MATLAB SIMULATOR

To support the analytical results developed in the previous section, we adapt LR-FHSS MATLAB® from (ULLAH *et al.*, 2022a; ULLAH *et al.*, 2022b) to encompass both the NC operation and the erasure probability. The flowchart of the updated simulator is presented in Fig. 4, where the main changes are highlighted in red and described in what follows:

- The headers of δ packets are linearly combined, generating an amount of δN_{H} coded-headers.
- Besides the collision, a packet element (either a coded-header or a payload fragment) can also be lost in case of erasure, when the channel is not in favorable conditions for transmission.
- At the GW side, besides counting the number of received payload fragments (depicted as F_{rx} in Fig. 4), the receiver also needs to evaluate the number of received coded-headers H_{rx}, declaring all the δ packets as lost when $H_{\text{rx}} < \delta$.

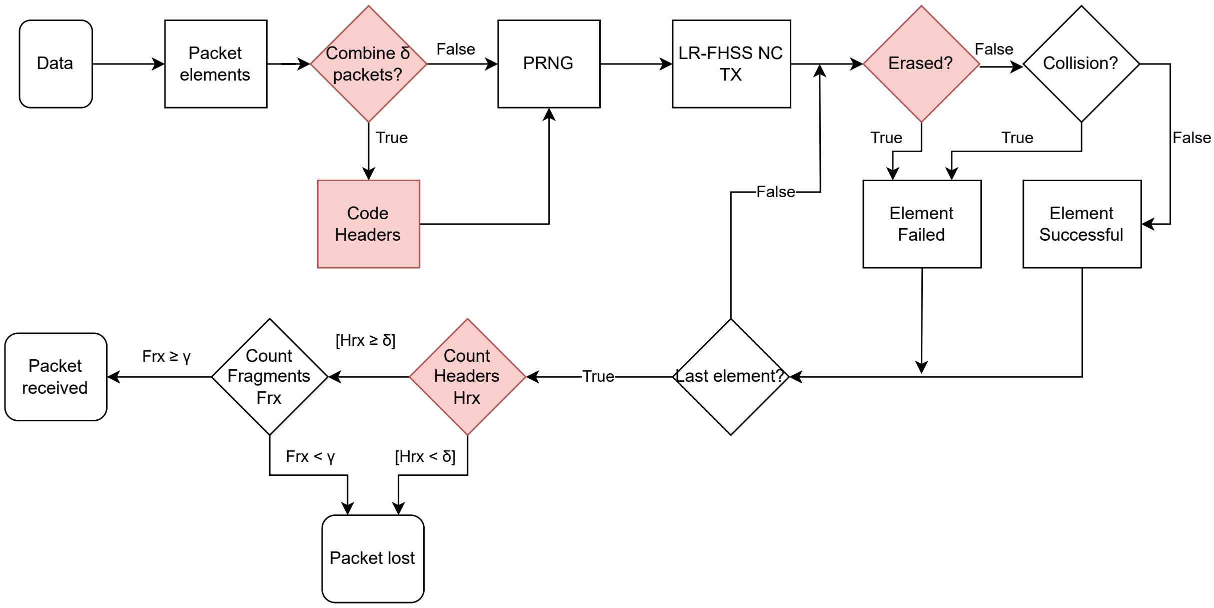

Figure 4 – LR-FHSS-NC simulator flowchart, adapted from the LR-FHSS model from (ULLAH *et al.*, 2022a).

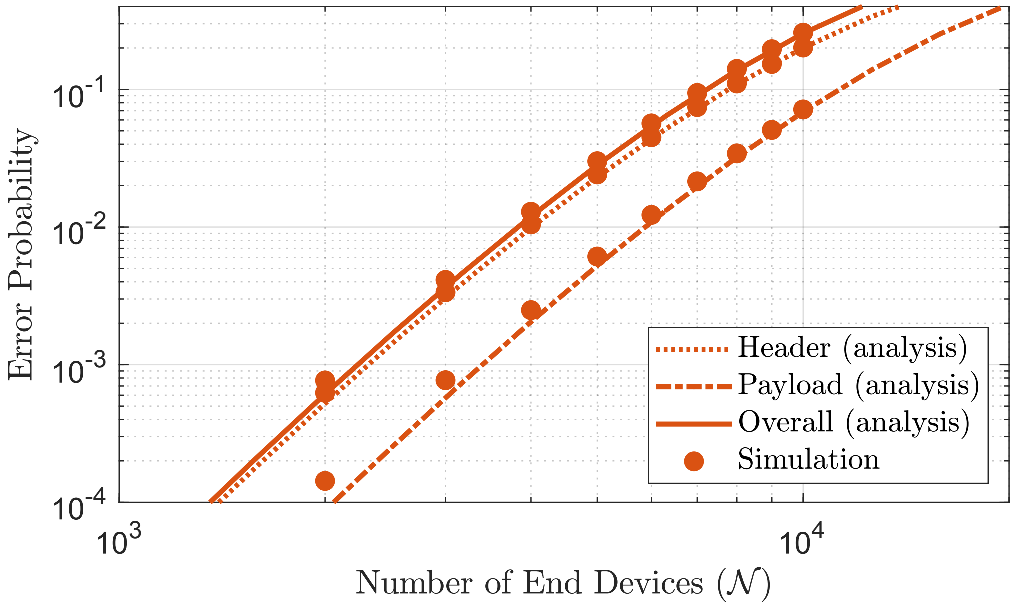

Figure 5 – Error probability of header, payload, and overall packet as a function of the number of end-devices $\mathcal{N}$, considering DR8, PL = 10 bytes and combining $\delta = 2$ header.

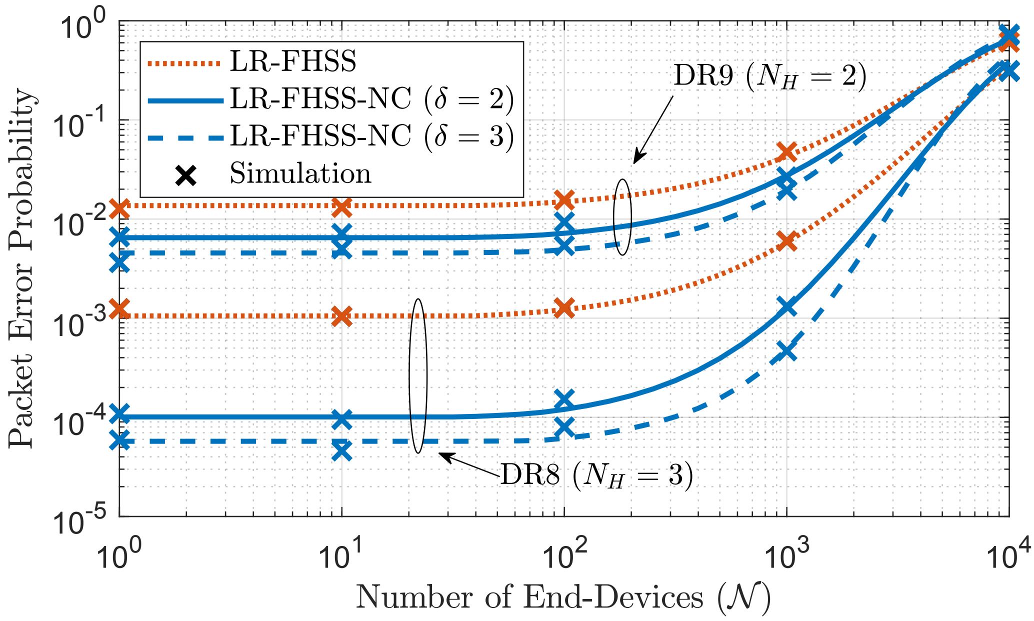

Figure 6 – Packet error probability versus number of end-devices, for $\delta \in \{2,3\}$, $N_{\mathsf{H}} \in \{2,3\}$ and $\epsilon = 0.1$.

5 NUMERICAL RESULTS

In this section, we present some numerical results to evaluate the performance of the proposed LR-FHSS-NC. Throughout the analysis, unless stated otherwise, we employ the ETSI parameters as detailed in Table 1, with packet payloads set to $\mathsf{PL} = 10$ bytes.

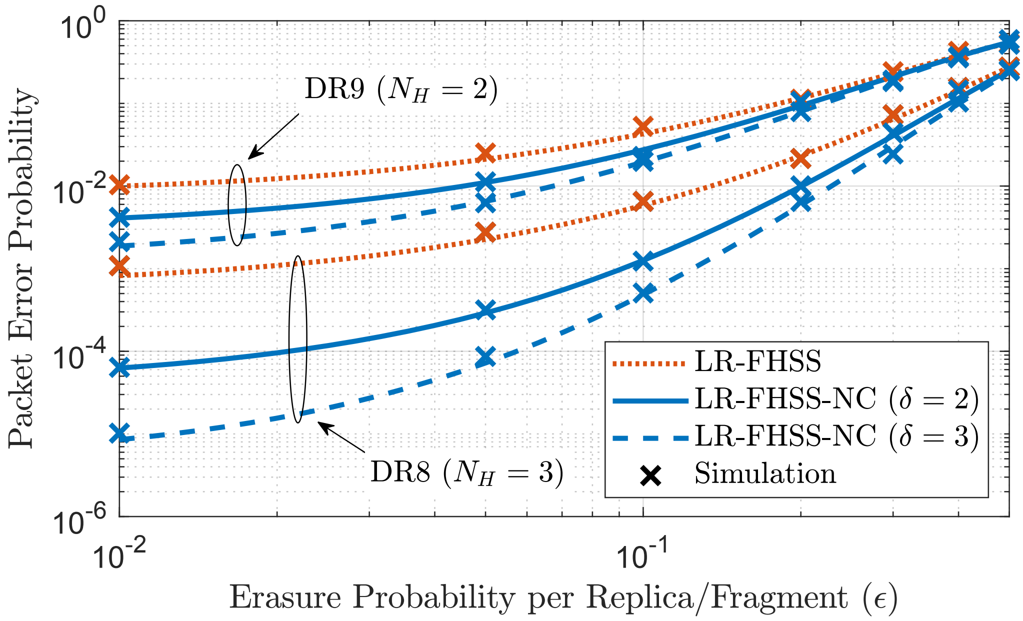

Figure 7 – Packet error probability versus erasure probability, for $\delta \in \{2,3\}$, $N_\mathrm{H} \in \{2,3\}$ and $\mathcal{N} = 1000$ EDs.

Fig. 6 shows the substantial gains achieved by the proposed LR-FHSS-NC scheme compared to standard LR-FHSS concerning packet error probability (PEP) against varying end-device counts ($\mathcal{N}$) for both DR8 and DR9, incorporating different values of δ while assuming an erasure probability $\epsilon = 0.1$. Notably, the advantage of LR-FHSS-NC over LR-FHSS is prominent, especially for DR8, demonstrating nearly an order of magnitude improvement for $\delta = 2$ across a wide spectrum of $\mathcal{N}$. Even for DR9, LR-FHSS-NC, particularly with $\delta = 2$, exhibits a remarkable $\sim 50\%$ enhancement over the benchmark LR-FHSS. Interestingly, it is also noteworthy that as δ increases, the gained improvement does not follow a linear progression; instead, the most significant gains are evident with smaller δ values. Moreover, the striking coherence between the simulation outcomes and the analytical projections further bolsters the credibility and reliability of the proposed scheme's performance evaluation.

Fig. 7 investigates the effect of erasure probability (ϵ) while considering a fixed number of $\mathcal{N} = 1000$ end-devices. As expected, the superiority of LR-FHSS-NC diminishes with higher ϵ values. However, it is intriguing to note that in scenarios typical of satellite networks, characterized by lower ϵ due to prevalent LOS conditions (MALEKI *et al.*, 2023a), LR-FHSS-NC demonstrates a substantial performance leap over LR-FHSS. Similar to the observations in Fig. 6, the superiority of LR-FHSS-NC is more pronounced for DR8. The increased number of header replicas in DR8 significantly enhances the error-correcting coding performance, contributing to the scheme's heightened advantage over the standard LR-FHSS.

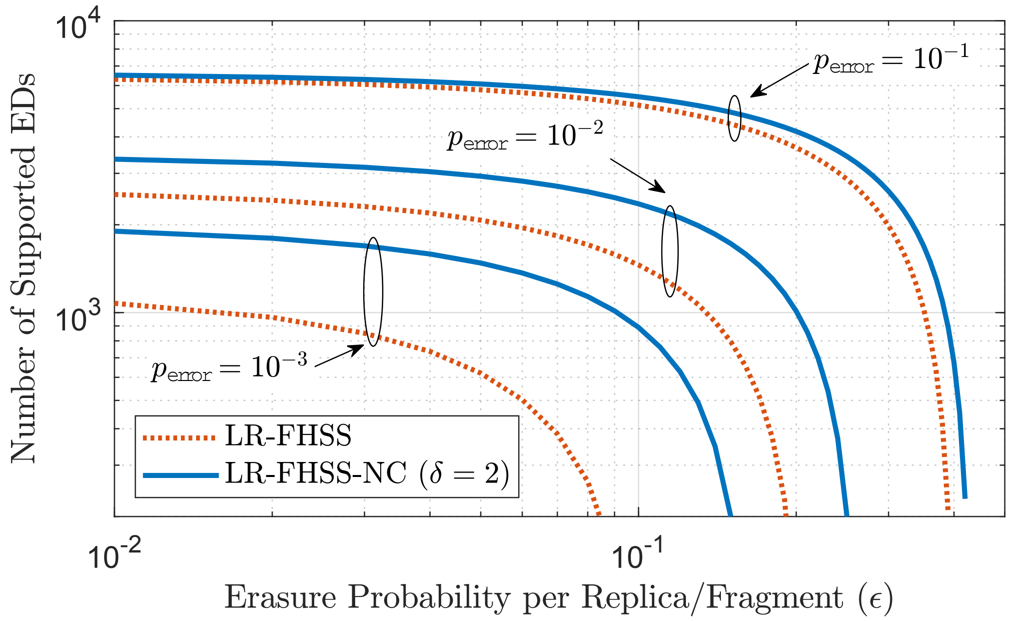

Figure 8 – Number of supported devices versus the erasure probability ϵ, for different target error probabilities $p_{\text{error}} \in \{10^{-3}, 10^{-2}, 10^{-1}\}$ and $\delta = 2$, $N_{\text{H}} = 3$, for DR8.

Fig. 8, focusing on DR8, explores the number of supported EDs concerning various erasure probability (ϵ) levels while setting the target Packet Error Probability (PEP) to $p_{\text{error}} \in 10^{-3}, 10^{-2}, 10^{-1}$. This analysis determines the highest number of EDs at which PEP $< p_{\text{error}}$. Notably, LR-FHSS-NC, particularly with $\delta = 2$, exhibits a more pronounced advantage when stringent PEP requirements are stipulated. Even with relatively high PEP values, such as 10^{-1} with $\epsilon = 0.3$, the proposed scheme supports 2600 EDs, marking approximately a 30% increase compared to the 2000 EDs supported by LR-FHSS

Particularly, the proposed scheme introduces an additional delay to the system as the headers of δ packets necessitate proper combination before transmission. In scenarios where sporadic transmission of a single packet occurs, with an average time between consecutive transmissions $T \gg \text{ToA}$, the first packet experiences a delay of $(\delta - 1)T$, the second packet $(\delta - 2)T$, and so forth until the last packet encounters no extra delay. Consequently, the average delay across these packets would be $(\delta - 1)T/2$. However, considering that LR-FHSS is frequently employed in satellite communications, typically associated with considerable latency (LEYVA-MAYORGA *et al.*, 2020), we believe that the additional delay imposed by LR-FHSS-NC would not hinder its practicality. Additionally, in scenarios where T is small, implying the transmission of multiple packets in bursts, the delay introduced by the proposed scheme becomes negligible.

6 CONCLUSION

In this thesis, we introduced an inter-header coding paradigm, the so-called LR-FHSS-NC, to increase the header success probability within LR-FHSS networks. The proposed LR-FHSS-NC scheme incorporates the combination of headers from multiple packets utilizing MDS codes, operating within a challenging environment susceptible to both collisions and erasures. Our analytical and simulation-based investigations reveal the substantial reduction in packet error probabilities achievable through the proposed scheme.

Moving forward, our future endeavors will encompass an assessment of LR-FHSS-NC's performance within a satellite constellation framework, involving multiple receivers and the synchronization challenges for cooperation. Further exploration will involve a comprehensive evaluation of the imposed delay by the LR-FHSS-NC scheme across various scenarios, enriching our understanding of its operational dynamics.

BIBLIOGRAPHY

AHMED, M.; HUQ, A.; AL-FUQAHA, A. A survey of network protocols for internet of things. **IEEE Internet of Things Journal**, v. 6, n. 6, p. 11914–11967, 2019.

AL-FUQAHA, A.; GUIZANI, M.; MOHAMMADI, M.; ALEDHARI, M.; AYYASH, M. Internet of things: A survey on enabling technologies, protocols, and applications. **IEEE Communications Surveys & Tutorials**, v. 17, n. 4, p. 2347–2376, 2015.

ALVES, Luis Henrique de Oliveira; REBELATTO, João Luiz; SOUZA, Richard Demo; BRANTE, Glauber. Network-Coded Cooperative LoRa Network With D2D Communication. **IEEE Internet of Things Journal**, v. 9, n. 7, p. 4997–5008, 2022.

ATZORI, L.; IERA, A.; MORABITO, G. The Internet of Things: A survey. **Computer Networks**, v. 54, n. 15, p. 2787–2805, 2010. ISSN 1389-1286. Disponível em: https://www.sciencedirect.com/science/article/pii/S1389128610001568. Acesso em: 01 jul. 2021.

ATZORI, Luigi; IERA, Antonio; MORABITO, Giacomo. From "smart objects" to "social objects": The next evolutionary step of the internet of things. **IEEE Communications Magazine**, v. 52, n. 1, p. 97–105, 2014.

BOQUET, Guillem; TUSET-PEIRÓ, Pere; ADELANTADO, Ferran; WATTEYNE, Thomas; VILAJOSANA, Xavier. LR-FHSS: Overview and Performance Analysis. **IEEE Commun. Mag."**, v. 59, n. 3, p. 30–36, 2021.

BORGIA, E. The internet of things vision: Key features, applications and open issues. **Computer Communications**, v. 54, n. 1, p. 1–31, 2014.

CHEN, M.; HAO, Y.; LI, H.; HU, L. Towards 6g wireless communication networks: Vision, architecture, technologies, and prospects. **IEEE Access**, v. 6, p. 36165–36175, 2018.

GEORGIOU, O.; RAZA, U. Low Power Wide Area Network Analysis: Can LoRa Scale? **IEEE Wireless Commun. Lett.**, v. 6, n. 2, p. 162–165, Apr. 2017. ISSN 2162-2337.

HOELLER, A.; SOUZA, R. D.; LóPEZ, O. L. Alcaraz; ALVES, H.; NETO, M. de Noronha; BRANTE, G. Analysis and Performance Optimization of LoRa Networks With Time and Antenna Diversity. **IEEE Access**, v. 6, p. 32820–32829, Jun. 2018. ISSN 2169-3536.

IKPEHAI, A.; ADEBISI, B.; RABIE, K. M.; ANOH, K.; ANDE, R. E.; HAMMOUDEH, M.; GACANIN, H.; MBANASO, U. M. Low-Power Wide Area Network Technologies for

Internet-of-Things: A Comparative Review. **IEEE Internet Things J.**, v. 6, n. 2, p. 2225–2240, Apr. 2019. ISSN 2372-2541.

JUNG, Sooyeob; JEONG, Seongah; KANG, Jinkyu; RYU, Joon Gyu; KANG, Joonhyuk. Transceiver design and performance analysis for lr-fhss-based direct-to-satellite iot. **IEEE Communications Letters**, v. 27, n. 12, p. 3310–3314, 2023.

KASSAB, Rahif; SIMEONE, Osvaldo; MUNARI, Andrea; CLAZZER, Federico. Space diversity-based grant-free random access for critical and non-critical iot services. *In*: **ICC 2020 - 2020 IEEE International Conference on Communications (ICC)**. *[S.l.: s.n.]*, 2020. p. 1–6.

KNOP, Diogo Nogueira; REBELATTO, João Luiz; SOUZA, Richard Demo. LR-FHSS With Network-Coded Header Replication. **IEEE Transactions on Vehicular Technology**, v. 73, n. 6, p. 9066–9070, 2024.

LEYVA-MAYORGA, Israel; SORET, Beatriz; RöPER, Maik; WüBBEN, Dirk; MATTHIESEN, Bho; DEKORSY, Armin; POPOVSKI, Petar. LEO Small-Satellite Constellations for 5G and Beyond-5G Communications. **IEEE Access**, v. 8, p. 184955–184964, 2020.

LIN, Shu; COSTELLO, Daniel J. **Error control coding: fundamentals and applications**. 2nd ed. ed. Upper Saddle River, N.J: Pearson-Prentice Hall, 2004. OCLC: ocm54952996. ISBN 9780130426727 9780130179739.

LORA ALLIANCE, INC. **LoRaWAN™ 1.1 Specification**. *[S.l.]*, 2017. Rev. 1.1. Disponível em: lora-alliance.org/wp-content/uploads/2020/11/lorawantm_specification_-v1.1.pdf.

LORA ALLIANCE, INC. **LoRaWAN® Regional Parameters**. *[S.l.]*, 2021. Rev. 1.0.3. Disponível em: https://lora-alliance.org/wp-content/uploads/2021/05/RP002-1.0.3-FINAL-1.pdf.

MAHMOOD, A.; SISINNI, E.; GUNTUPALLI, L.; RONDÓN, R.; HASSAN, S. A.; GIDLUND, M. Scalability Analysis of a LoRa Network Under Imperfect Orthogonality. **IEEE Trans. Ind. Informat.**, v. 15, n. 3, p. 1425–1436, Mar. 2019. ISSN 1551-3203.

MALEKI, Alireza; NGUYEN, Ha H.; BARTON, Robert. Outage Probability Analysis of LR-FHSS in Satellite IoT Networks. **IEEE Communications Letters**, v. 27, n. 3, p. 946–950, 2023.

MALEKI, Alireza; NGUYEN, Ha H.; BEDEER, Ebrahim; BARTON, Robert. Outage probability analysis of lr-fhss and d2d-aided lr-fhss protocols in shadowed-rice fading direct-to-satellite iot networks. **IEEE Internet of Things Journal**, p. 1–1, 2023.

MUNARI, Andrea; CLAZZER, Federico; LIVA, Gianluigi; HEINDLMAIER, Michael. Multiple-relay slotted aloha: Performance analysis and bounds. **IEEE Transactions on Communications**, v. 69, n. 3, p. 1578–1594, 2021.

NOLAN, Keith E.; GUIBENE, Wael; KELLY, Mark Y. An evaluation of low power wide area network technologies for the internet of things. *In*: **2016 International Wireless Communications and Mobile Computing Conference (IWCMC)**. *[S.l.: s.n.]*, 2016. p. 439–444.

RAZA, U.; KULKARNI, P.; SOORIYABANDARA, M. Low Power Wide Area Networks: An Overview. **IEEE Commun. Surveys Tuts.**, v. 19, n. 2, p. 855–873, Secondquarter 2017.

REBELATTO, João Luiz; UCHÔA-FILHO, Bartolomeu F.; LI, Yonghui; VUCETIC, Branka. Multi-User Cooperative Diversity through Network Coding Based on Classical Coding Theory. **IEEE Trans. Signal Process.**, v. 60, n. 2, p. 916–926, Feb. 2012.

REED, I. S.; SOLOMON, G. Polynomial codes over certain finite fields. **SIAM Journal of Applied Mathematics**, v. 8, p. 300–304, 1960.

SANT'ANA, Jean; JR, Arliones Hoeller; SOUZA, Richard; SÁNCHEZ, Samuel Montejo; ALVES, Hirley; NETO, Mario. Hybrid Coded Replication in LoRa Networks. **IEEE Trans. Ind. Informat.**, v. 16, n. 8, p. 5577–5585, Aug. 2020.

SANT'ANA, J. M. de Souza; HOELLER, A.; SOUZA, R. D.; ALVES, H.; MONTEJO-SáNCHEZ, S. LoRa Performance Analysis with Superposed Signal Decoding. **IEEE Wireless Commun. Lett.**, v. 9, n. 11, p. 1865–1868, Nov. 2020.

Olivier Bernard André Seller. **Wireless Communication Method**. 2017. 9 647 718.

SEMTECH CORPORATION. **SX1272/73 - 860 MHz to 1020 MHz Low Power Long Range Transceiver**. Wireless & Sensing Products, 2019. Rev. 4.

SUNDARAM, J. P. Shanmuga; DU, W.; ZHAO, Z. A Survey on LoRa Networking: Research Problems, Current Solutions, and Open Issues. **IEEE Commun. Surveys Tuts.**, v. 22, n. 1, p. 371–388, Firstquarter 2020. ISSN 2373-745X.

TEMIM, Mohamed Amine Ben; FERRé, Guillaume; SELLER, Olivier. An lr-fhss receiver for a massive iot connectivity. *In*: **2023 IEEE 34th Annual International Symposium on Personal, Indoor and Mobile Radio Communications (PIMRC)**. *[S.l.: s.n.]*, 2023. p. 1–6.

ULLAH, Muhammad Asad; MIKHAYLOV, Konstantin; ALVES, Hirley. Analysis and Simulation of LoRaWAN LR-FHSS for Direct-to-Satellite Scenario. **IEEE Wireless Communications Letters**, v. 11, n. 3, p. 548–552, 2022.

ULLAH, Muhammad Asad; MIKHAYLOV, Konstantin; ALVES, Hirley. **Analysis-and-Simulation-of-LoRaWAN-LR-FHSS. Github**. 2022. Disponível em: https://github.com/MuhammadAsadUllah1/Analysis-and-Simulation-of-LoRaWAN-LR-FHSS.git.

XIAO, Ming; SKOGLUND, Mikael. Multiple-User Cooperative Communications Based on Linear Network Coding. **IEEE Trans. Commun.**, v. 58, n. 12, p. 3345–3351, Dec. 2010.

ZHANG, Fanhao; YU, Fu; ZHENG, Xiaolong; LIU, Liang; MA, Huadong. Dfh: Improving the reliability of lr-fhss via dynamic frequency hopping. *In*: **2023 IEEE 31st International Conference on Network Protocols (ICNP)**. *[S.l.: s.n.]*, 2023. p. 1–12.

ÁLVAREZ, Guido; FRAIRE, Juan A.; HASSAN, Khaled Abdelfadeel; CéSPEDES, Sandra; PESCH, Dirk. Uplink Transmission Policies for LoRa-Based Direct-to-Satellite IoT. **IEEE Access**, v. 10, p. 72687–72701, 2022.

APPENDIX

APPENDIX A – FADING MODEL

The On-Off fading model is a stochastic representation of wireless communication channels. It characterizes the channel's behavior by alternating between two distinct states: an "On" state, signifying good or available channel conditions suitable for communication, and an "Off" state, representing instances where the channel is unusable or impaired.

Specifically relevant for IoT applications using Low Earth Orbit (LEO) satellites, this model describes the link between users and relays in a dual-state fashion, reflecting the intermittent availability of the channel due to fading or interference (MUNARI *et al.*, 2021). Its accuracy in depicting the behavior of ALOHA-based schemes, especially in scenarios with complex channel conditions like Rayleigh fading or power imbalances, makes it an ideal reference in numerous studies focusing on random access methods for IoT (MUNARI *et al.*, 2021).

Certainly, it's crucial to acknowledge the multifaceted nature of the erasure probability, contingent upon diverse factors like device proximity to the satellite, carrier frequency, antenna characteristics, data rate, and environmental hindrances. Determining the precise erasure probability involves analyzing outage probabilities, a complex task necessitating comprehensive information.

In this work, the focus remains on furnishing analytical tools to assess packet error probabilities tailored for specific network setups, encompassing variables such as device count and data rates. The methods for deriving these probabilities are elucidated in Section 4.2 of the manuscript, steering clear of calculating precise erasure probabilities for individual setups, a task beyond the scope of this study and the related literature.

In prior studies, such as references (ULLAH *et al.*, 2022a; MALEKI *et al.*, 2023a), the use of the Ricean and Nakagami-m distributions has been instrumental in evaluating the capture effect within collision scenarios, particularly concerning the potential recovery of collided packets based on the signal to interference ratio surpassing a predefined threshold. However, while (ULLAH *et al.*, 2022a) solely relied on simulations to explore the capture effect, deriving practical insights from the intricate analytical model proposed in (MALEKI *et al.*, 2023a) proved challenging.

A critical gap prevalent in both studies is the absence of a specified capture threshold tailored explicitly for LR-FHSS networks. Notably, such a threshold should differ for header replicas and payload fragments in LR-FHSS due to the distinct application of error correcting codes. Presently, no academic literature, standard specifications, or datasheets offer a defined capture threshold specific to LR-FHSS, complicating its accurate assessment.

An observation drawn from (MALEKI *et al.*, 2023a) underscores that even a single interfering device could lead to a notably high probability of signal loss. This observation aligns with the approach adopted in our work, where the collision resolution within LR-FHSS inherently results in the irrevocable loss of a packet element upon concurrent transmission with another device's packet.

Nevertheless, for clarity, we align our work with the Nakagami-m channel model employed in (MALEKI *et al.*, 2023a). This model, encompassing the satellite-suitable path loss and noise characteristics, serves to substantiate our argument that while the On-Off channel model offers mathematical tractability, it doesn't compromise generality.

In the context of (MALEKI *et al.*, 2023a), the term 'disconnection' denotes scenarios where the signal-to-noise ratio (SNR) for receiving a packet element falls below a defined threshold (ψ). This 'disconnection probability' within their context essentially corresponds to the erasure probability parameter employed in our work.

Building upon the insights from (MALEKI *et al.*, 2023a, Eq. (12)), the disconnection probability for a packet element experiencing Nakagami-m fading can be mathematically expressed as:

$$P_{\text{disc}} = \frac{1}{\Gamma(m)}\,\gamma\left(m, \frac{m\,\psi\,\sigma^2}{P}\,g(\alpha)\right), \tag{18}$$

where m is the Nakagami-m parameter, $\Gamma(\cdot)$ the complete gamma function, $\gamma(a,b)$ the unnormalized incomplete Gamma function, P the effective received power (encompassing transmit power and antenna gains), ψ the SNR threshold of the satellite receiver and $\sigma^2 = -174 + \text{NF} + 10\log 10(B)$ the AWGN variance (in dBm), being NF the noise figure (dB) and B the bandwidth (Hz). In (18), $g(\alpha)$ represents the satellite path loss for a given elevation angle α, obtained (in dB) as (MALEKI *et al.*, 2023a, Eq. (3))

$$g(\alpha) = 32.44 + 20\log(d(\alpha)) + 20\log(f) + L_{\text{air}}(\alpha) + L_{\text{rain}} + L_{\text{tree}}(\alpha) + L_{\text{fog}} + L_{\text{iono}} + L_{\text{frad}}, \tag{19}$$

where $d(\alpha)$, f, L_{air}, L_{rain}, L_{tree}, L_{fog}, L_{iono} and L_{frad} denote respectively the distance to the satellite (in km), carrier frequency (in MHz), absorption of the atmosphere, attenuation caused by rain (absorption and scattering), tree, cloud or fog, ionosphere and polarization effects, respectively. The distance $d(\alpha)$, in turn, is calculated (in km) as (MALEKI *et al.*, 2023a, Eq. (4))

$$d(\alpha) = R\left(\sqrt{\left(\frac{H+R}{R}\right)^2 - \cos^2(\alpha)} - \sin(\alpha)\right), \tag{20}$$

Table 4 – Parameters adopted to reproduce the results from Figure 9, obtained from (MALEKI *et al.*, 2023a; ÁLVAREZ *et al.*, 2022).

Parameter	Symbol	Value
Elevation angle	α	10 : 1 : 90 degrees
Nakagami fading parameter	m	$\in \{2,3,4\}$
Satellite orbital height	H	780 km
LR-FHSS transmitted power	P_t	14 dBm
Transmitter antenna gain	G_t	2.5 dBi
Receiver antenna gain	G_r	16 dBi
LR-FHSS bandwidth	B	488 Hz
Carrier frequency	f	905.4385 MHz
LR-FHSS receiver threshold	ψ	3.96 dB
Noise figure	NF	6 dB

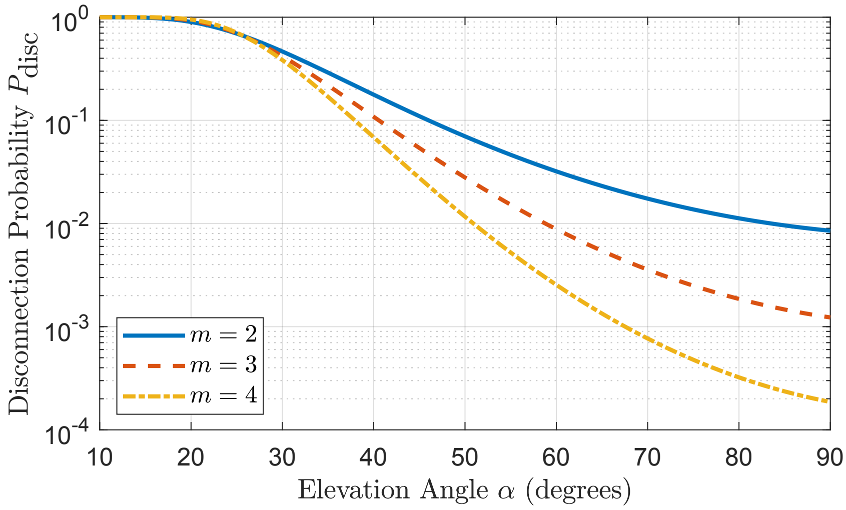

Figure 9 – Disconnection probability versus the elevation angle, for different values of $m \in \{2,3,4\}$ and parameters presented in Table 4, obtained from (MALEKI *et al.*, 2023a; ÁLVAREZ *et al.*, 2022).

where $H = 780$ km is the orbital height of the satellite, and $R = 6378$ km is the Earth radius, while the values for other path-loss parameters (in dB) can be set as (MALEKI *et al.*, 2023a): $L_{\text{air}}(\alpha) = 0.1(1 + \cos(\alpha))$, $L_{\text{rain}} < 0.1$, $L_{\text{fog}} = 0$, $L_{\text{iono}} + L_{\text{frad}} = 3$, and (MALEKI *et al.*, 2023a, Eq. (5))

$$L_{\text{tree}}(\alpha) = \sqrt{\frac{f}{900}} \left[25.8 \exp\left(-1.1 \frac{1.57\alpha}{90} \right) + 1.5 \cos\left(\frac{3.937\alpha}{90} \right) \right]. \tag{21}$$

Utilizing the parameters outlined in Table 4, sourced from studies by (MALEKI *et al.*, 2023a; ÁLVAREZ *et al.*, 2022), the disconnection probability is computed across various Nakagami parameters m by altering the elevation angle α, which corresponds to varying the distance between the device and the satellite. The resulting disconnection probabilities are graphically represented in Figure 9.

The observations drawn from Fig. 9 highlight a correlation between specific configurations and resulting disconnection probabilities. For instance, when considering $\alpha = 40°$ and $m = 3$, the obtained P_{disc} approximately aligns with the designated value of $\epsilon = 0.1$ utilized in our On-Off scenario, as depicted, for instance, in Fig. 6. Similarly, distinct setups, such as $\alpha = 50^\circ$ and $m = 4$, are associated with different erasure probabilities, like $\epsilon = 10^{-2}$, and so forth. This showcases a potential mapping between specific Nakagami parameters and elevation angles to the corresponding erasure probabilities utilized in our simulations.

APPENDIX B – ARITHMETIC OPERATIONS OVER A FINITE FIELD

In a finite field, arithmetic operations such as addition, subtraction, multiplication, and division are conducted within a limited set of elements, typically represented as GF(q), where q is a prime number or a power of a prime number. Specifically, in the finite field GF(4), there exist four elements. The symbols $\boxplus$ and $\boxtimes$ signify addition and multiplication operations, respectively, within the finite field, as illustrated in Table 5.

For instance, let's consider a hypothetical scenario where s_1 and s_2 represent two messages, each containing 8 bits. We can express these messages in binary and in $GF(4)$ notation as follows:

$$s_1 = [0\ \ 1\ \ 1\ \ 1\ \ 1\ \ 0\ \ 0\ \ 1]_2 = [1\ \ 3\ \ 2\ \ 1\ \ ]_4$$
$$s_2 = [1\ \ 1\ \ 1\ \ 0\ \ 0\ \ 0\ \ 0\ \ 1]_2 = [3\ \ 2\ \ 0\ \ 1\ \ ]_4$$

We then utilize Table 5 to perform addition and multiplication operations on s_1 and s_2, yielding the following results:

$$\begin{aligned} s_1 \boxplus s_2 &= [1 \boxplus 3\ \ 3 \boxplus 2\ \ 2 \boxplus 0\ \ 1 \boxplus 1]_4 \\ &= [2\ \ 1\ \ 2\ \ 0]_4 \\ &= [1\ \ 0\ \ 0\ \ 1\ \ 1\ \ 0\ \ 0\ \ 0]_2 \end{aligned}$$

and

$$\begin{aligned} s_1 \boxtimes s_2 &= [1 \boxtimes 3\ \ 3 \boxtimes 2\ \ 2 \boxtimes 0\ \ 1 \boxtimes 1]_4 \\ &= [3\ \ 1\ \ 0\ \ 1]_4 \\ &= [1\ \ 1\ \ 0\ \ 1\ \ 0\ \ 0\ \ 0\ \ 1]_2 \end{aligned}$$

Furthermore, if we wish to multiply s_1 by a linear coefficient, 2, in $GF(4)$, the operation is carried out as follows:

$$\begin{aligned} 2 \boxtimes s_1 &= [2 \boxtimes 1\ \ 2 \boxtimes 3\ \ 2 \boxtimes 2\ \ 2 \boxtimes 1]_4 \\ &= [2\ \ 1\ \ 3\ \ 2]_4 \\ &= [1\ \ 0\ \ 0\ \ 1\ \ 1\ \ 1\ \ 1\ \ 0]_2 \end{aligned}$$

Table 5 – Operations (a) Addition and (b) Multiplication finite field GF(4).

$\boxplus$	0	1	2	3
0	0	1	2	3
1	1	0	3	2
2	2	3	0	1
3	3	1	1	0

a

$\boxtimes$	0	1	2	3
0	0	0	0	0
1	0	1	2	3
2	0	2	3	1
3	0	3	1	2

b

These operations demonstrate the application of addition, multiplication, and scalar multiplication within the finite field $GF(4)$, showcasing the versatility and applicability of finite field operations.